Published in final edited form as:
Biochemistry. 2013 August 27; 52(34): . doi:10.1021/bi4005649.

Binding of a Third Metal Ion by the Human Phosphatases PP2Cα and Wip1 is Required for Phosphatase Activity

Kan Tanoue, **Lisa M. Miller Jenkins**, **Stewart R. Durell**, **Subrata Debnath**, **Hiroyasu Sakai**, **Harichandra D. Tagad**, **Kazushige Ishida**, **Ettore Appella**, and **Sharlyn J. Mazur***
Laboratory of Cell Biology, National Cancer Institute, National Institutes of Health, Bethesda, Maryland 20892, United States

Abstract

The PPM phosphatases require millimolar concentrations of Mg^{2+} or Mn^{2+} to activate phosphatase activity in vitro. The human phosphatases PP2Cα (PPM1A) and Wip1 (PPM1D) differ in their physiological function, substrate specificity, and apparent metal affinity. A crystallographic structure of PP2Cα shows only two metal ions in the active site. However, recent structural studies of several bacterial PP2C phosphatases have indicated three metal ions in the active site. Two residues that coordinate the third metal ion are highly conserved, suggesting that human PP2C phosphatases may also bind a third ion. Here, isothermal titration calorimetry analysis of Mg^{2+} binding to PP2Cα distinguished binding of two ions to high affinity sites from the binding of a third ion with a millimolar affinity, similar to the apparent metal affinity required for catalytic activity. Mutational analysis indicated that Asp239 and either Asp146 or Asp243 was required for low-affinity binding of Mg^{2+}, but that both Asp146 and Asp239 were required for catalysis. Phosphatase activity assays in the presence of $MgCl_2$, $MnCl_2$, or mixtures of the two, demonstrate high phosphatase activity toward a phosphopeptide substrate when Mg^{2+} was bound to the low-affinity site, whether Mg^{2+} or Mn^{2+} ions were bound to the high affinity sites. Mutation of the corresponding putative third metal ion-coordinating residues of Wip1 affected catalytic activity similarly both in vitro and in human cells. These results suggest that phosphatase activity toward phosphopeptide substrates by PP2Cα and Wip1 requires the binding of a Mg^{2+} ion to the low-affinity site.

Protein phosphorylation by kinases and subsequent dephosphorylation by phosphatases is exploited in all three domains of life in forming signaling pathways, but is especially prominent in eukaryotes. Serine/threonine phosphatases are classified into the evolutionarily unrelated PPP and PPM superfamilies by sequence similarity, sensitivity to inhibitors, and metal-ion dependence (1-3). The PPM phosphatases are insensitive to okadaic acid, a potent inhibitor of the PPP family phosphatases, and require supplementation with millimolar concentrations of Mg^{2+} or Mn^{2+} for catalytic activity in vitro (1, 3). Analysis of PPM phosphatase protein sequences has identified 13 motifs conserved among the PP2C phosphatases, 11 of which are also conserved among the more-distantly related SpoIIE-type phosphatases (4). Seventeen genes encoding PP2C phosphatases have been identified in the

*Corresponding Author Address: 37 Convent Dr., Building 37 Room 2140, Bethesda, MD 20892. Telephone: (301) 435-6293. Fax: (301) 435-8188. mazurs@mail.nih.gov.

Supporting Information **Available**: Figure S1 displays RMSD values comparing the positions of 11 active site Cα atoms of PP2Cα (PDB 1A6Q) to the corresponding atoms of 34 PP2C or PPM phosphatases containing one, two, or three metal ions in the active site. Figure S2 displays ITC results characterizing the binding of Mg^{2+} to WT, D146A, D239A and D243A proteins. Figure S3 displays a multiple sequence alignment of the catalytic domains of 18 human PP2Cc-containing proteins. Figure S4 displays position-specific residue frequencies for active site residues among 134 PP2C catalytic domain sequences. Figure S5 depicts contacts between adjacent monomers in the PP2Cα crystal (PDB 1A6Q) that may affect M3-coordinating residue conformations. This material is available free of charge via the Internet at http://pubs.acs.org.

human genome (1-3, 5). Although the PP2C phosphatases account for a small portion of the protein phosphatase activity in eukaryotic cells, their activity is especially important in cellular stress signaling pathways that regulate cell growth, survival and apoptosis (1, 6).

PP2Cα (PPM1A) was the first member of the human PP2C family to be identified and remains the best-characterized (1). Wip1 (PPM1D) was first characterized as a gene induced by the p53 tumor suppressor after exposure of cells to DNA damaging agents, such as ionizing radiation (IR) and ultraviolet radiation (7). In general, both proteins are negative regulators of cellular stress-response pathways, but differ in their substrate specificity, patterns of tissue-specific expression, and character as a tumor suppressor or oncogene. Both proteins negatively regulate the Mitogen-Activated Protein Kinase (MAPK p38α) pathway through dephosphorylation of pThr180 of MAPK p38α (8, 9). Activation of MAPK p38α requires phosphorylation of both Thr180 and Tyr182 within its activation loop; removal of either modification inactivates the kinase (9). Based on in vitro phosphatase assays, PP2Cα had greater activity toward the monophosphorylated pThr (180) peptide, whereas Wip1 had greater activity toward the diphosphorylated peptide (10). PP2Cα activates the tumor suppressor p53 as a transcription factor, resulting in cell cycle arrest, increased apoptosis, and reduced tumorigenicity (1, 11). Conversely, Wip1 negatively regulates p53 by inactivating upstream kinases, including Ataxia telangiectasia mutated (ATM) and MAPK p38 (8, 12, 13), by reducing DNA-damage signaling through dephosphorylation of γH2AX (14-16), and by stabilizing MDM2, the major negative regulator of p53 stability (17). Thus, Wip1 has been shown to be an important negative regulator of several tumor suppressors, including p53 (18-20), whereas PP2Cα functions as a tumor suppressor protein through p53-dependent and -independent mechanisms (1, 11).

A crystal structure of PP2Cα was reported in 1996 (21). The catalytic domain of PP2Cα is formed by a β-sandwich consisting of two anti-parallel β-sheets with a pair of α-helices flanking each β-sheet. The active site was identified as a shallow groove containing two Mn^{2+} ions coordinated by water molecules and several highly-conserved aspartic acid residues (21). The catalytic mechanism has been elucidated as an instance of a binuclear metallohydrolase (21-23). In addition, PP2Cα has a small domain of unique structure, called a Flap domain, which is inserted between strands β8 and β9 of the catalytic domain (21, 24, 25). This domain, which spans conserved motifs 5a and 5b, is found in the PP2C phosphatases, the mitochondrial pyruvate dehydrogenase phosphatases (PDP), and the phosphatase domains of fungal adenylate cyclases, but is absent in bacterial SpoIIE-type phosphatases (4, 26). The function of the Flap domain is uncertain, but appears to be involved in substrate recognition (25, 27, 28).

The initial mechanism proposed for the catalytic activity of PP2Cα was based on the involvement of two metal ions (21, 22). Despite its other strengths, the mechanism did not provide an explanation for the observed requirement for millimolar concentrations of metal ions to activate phosphatase activity, as the two Mn^{2+} ions of PP2Cα observed in the crystal structure are bound with higher affinities. Recently, structural studies of several bacterial PP2C phosphatases revealed the presence of a third metal ion in the active site (24, 25, 28-31). Although catalytic mechanisms involving three metals have been proposed (28, 29), the function of the third metal ion remains controversial. As two of the residues coordinating the third metal ion are highly conserved, the involvement of a third metal ion in the catalytic mechanism was suggested to be a general characteristic of PP2C phosphatases (24). Accordingly, recent structural studies of two plant PP2C phosphatases have also revealed the presence of three metal ions in the active site (32-34).

In this study, we have investigated the millimolar-affinity binding of magnesium ions to human PP2Cα using site-directed mutagenesis, phosphatase activity assays, and isothermal

titration calorimetry (ITC). Our results provide a thermodynamic characterization of the binding of a third magnesium ion to PP2Cα, suggest that its binding is essential for catalytic activity, and provide further explanations for the absence of a third metal ion in crystals of PP2Cα grown at low pH. In addition, we show that mutation of the corresponding residues in Wip1 similarly abolished or reduced phosphatase activity both in vitro and in human cells. Analysis of the conservation of active site residues suggests that the involvement of a third metal ion in the catalytic mechanism is likely to be a feature common to many of the human PP2C phosphatases.

Experimental procedures

Expression vectors

PP2Cα cDNA was cloned into the BamHI-KpnI sites of the pET45b(+) vector by PCR using the following oligonucleotide primers: 5′-ACGTGGGTACCATGGGAGCATTTTTAGACAAGC-3′ and 5′-AATTGGGATCCTTACCACATATCATCTGTTGATGTAGAGTC-3′ (pET45b(+)-His-PP2Cα). To generate a vector expressing the fusion protein with a Tobacco Etch Virus (TEV) protease site inserted between the 6×His tag and PP2Cα (pET45b(+)-His-TEV-PP2Cα), the oligonucleotide duplex formed by 5′-GTACGGGAGAAAACCTGTACTTCCAGTCAGGAG-3′ and 5′-GTACCTCCTGACTGGAAGTACAGGTTTTCTCCC-3′ was phosphorylated using T4 polynucleotide kinase and cloned into Acc65I-digested pET45b(+)-His-PP2Cα. To generate a vector expressing the catalytic domain of Wip1 as a fusion protein with an N-terminal 6×His-ProS2 domain (pCold-His-ProS2-Wip1(1-420)), Wip1 cDNA was cloned into the NdeI and HindIII sites of the pCold-ProS2 vector (TAKARA) vector by PCR using the following oligonucleotide primers: 5′-GGAATTCCATATGGCGGGGCTGTACTCGCTG-3′, 5′-CCCAAGCTTACTTGACTGGTGGTGTAGAACATG-3′. Vectors to express WT and D314A Wip1 in mammalian cells were obtained from Addgene (plasmids 28105 and 28106) (35); the corresponding parental vector, pCMV-Neo-Bam, has been described (36). Point mutations were introduced into bacterial or mammalian expression vectors using the Quickchange II or Quickchange II XL Mutagenesis Kit (Agilent) and verified by sequencing.

Protein expression and purification

All proteins were expressed in *E. coli* BL21(DE3). pET45b(+)-His-PP2Cα, pET45b(+)-His-TEV-PP2Cα and derived mutant vectors were grown in Luria-Bertani broth (LB) at 37 °C and induced with 0.1 mM isopropyl-1-thio-β-d-galactopyranoside (IPTG) at 30 °C overnight. Upon induction, 1 mM $MnCl_2$ was added to the LB. Cell pellets expressing wildtype (WT) or mutant His-PP2Cα were resuspended in Buffer A (phosphate-buffered saline (PBS), 2 mM 2-Mercaptoethanol (β-ME), 10% glycerol, 0.2% Triton X-100 and Ethylenediaminetetraacetic acid (EDTA)-free protease inhibitor cocktail tablets (Roche)) supplemented with 2 mM $MnCl_2$ and lysed by sonication. The lysate was centrifuged at 13000 × *g* to pellet cellular debris and the supernatant was incubated with TALON metal affinity resin (Clontech) equilibrated with Buffer B (PBS with 500 mM NaCl, 1 mM β-ME and 10% glycerol) for 1 h at 4 °C. The resin was then washed by gravity flow with 16-20 column volumes of Buffer B followed by 16-20 column volumes of Buffer C (50 mM tris(hydroxymethyl)aminomethane (Tris)-HCl (pH 7.5), 0.02% β-ME, 0.1 mM ethylene glycol tetraacetic acid (EGTA)) with 5 mM imidazole. His-tagged protein was eluted with Buffer C plus 150 mM imidazole. Peak fractions were dialyzed against Buffer C plus 10% glycerol for 1 h and again overnight in fresh buffer to remove imidazole. The dialysis buffer for PP2Cα R186A mutant contained, in addition, 2 mM $MnCl_2$. Cell pellets expressing WT

and mutant His-TEV-PP2Cα were resuspended in Buffer D (50 mM 4-2-hydroxyethyl-1-piperazineethanesulfonic acid (HEPES) (pH 7.5), 150 mM NaCl, 2 mM $MgCl_2$, 2 mM β-ME, 10% glycerol, and 0.1 mM EGTA) with EDTA-free protease inhibitor cocktail (Roche) and 0.2% Triton X-100 and lysed by sonication. The lysate was centrifuged at 13000 × *g*. His-TEV-PP2Cα protein contained in the supernatant was purified by TALON metal affinity chromatography as described above except that Buffers B and C were replaced by Buffer D, with addition of 5 mM or 150 mM imidazole for the corresponding steps. Following overnight dialysis against Buffer D, the His-TEV-PP2Cα-containing fraction was incubated with TEV protease for 2 h at 30 °C, and then incubated with TALON metal affinity resin equilibrated with Buffer D to remove the cleaved His-tag. For WT and mutant proteins prepared by the EDTA method, the unbound protein and peak fractions collected after a Buffer D wash were pooled and dialyzed against ITC buffer (50 mM HEPES (pH 7.5), 150 mM NaCl, 10% glycerol, 2 mM β-ME) supplemented with 5 mM EDTA for 1 h, four times, followed by ITC buffer for 1 h, two times, and then overnight. For WT and mutant proteins prepared by the dialysis method, purified proteins supplemented with 8 to 30 mM $MgCl_2$ were dialyzed against ITC buffer for 1 h, two times, and then overnight. For additional ITC analysis of WT PP2Cα, dialysis buffers were treated with Chelex-100 resin, as specified in the text.

Cultures of pCold-His-ProS2-Wip1(1-420) and mutants were grown in LB at 30 °C and induced with 0.25 mM IPTG overnight at 15 °C. Cell pellets were resuspended in Buffer A and lysed by French press. Following removal of cellular debris by centrifugation, the protein was purified by the same method as His-PP2Cα, except that the TALON metal affinity column containing the bound protein was washed sequentially by Buffer B (16-20 column volumes), Buffer C with 5 mM imidazole (16-20 column volumes), and Buffer C with 150 mM imidazole (6 column volumes). His-tagged ProS2-Wip1(1-420) was eluted with Buffer C plus 400 mM imidazole, and peak fractions were dialyzed as described above. All purified proteins were at least 95% pure as determined by gel electrophoresis followed by staining with Simply Blue Safe Stain (Invitrogen).

Steady-state kinetics assays

The sequence of the synthetic human p38α (175-185)(180pT) peptide used as substrate is NH_2-TDDEMpTGYVAT-COOH. Phosphatase activity toward the phosphopeptide substrate was measured by a Biomol green-based assay (Enzo Life Science), following the manufacturer's protocol. For determination of the initial rates of phosphatase activity, 15 ng of WT or mutant His-PP2Cα were incubated with various concentrations of human p38α (175-185)(180pT) peptide and $MgCl_2$ in Buffer C plus 40 mM NaCl at 30 °C for 9 min. For determination of the metal dependence of activity, $MnCl_2$, $CaCl_2$, or $ZnCl_2$ was substituted for $MgCl_2$. In addition, some experiments were performed under the same conditions using WT or mutant PP2Cα from which the 6×His tag had been removed. Initial rates of reaction for WT or mutant His-ProS2-Wip1 were determined similarly, except that 60 ng of protein was used and the reaction was allowed to proceed for 7 min. Phosphatase activity toward *p*-nitrophenyl phosphate (pNPP) was measured under the same conditions described above except that 120 ng of His-PP2Cα and the indicated concentrations of $MnCl_2$ were used. The assay was terminated by adding NaOH and EDTA. The amount of *p*-nitrophenol released was determined spectrophotometrically (ε = 18000 M^{-1} cm^{-1} at 410 nm). For determination of the pH dependence of the activity, 50 mM Tris-HCl (pH 6.5) or 50 mM MES-NaOH (pH 5.0) were used in place of 50 mM Tris-HCl (pH 7.5). The initial rates were fitted to the Michaelis-Menten equation (Equation 1) to determine the K_m and V_{max} values,

$$\nu = V_{\max}[S]/(K_m + [S]), \quad [1]$$

where [*S*] is the concentration of substrate. The value of k_{cat} was calculated from $V_{max} = k_{cat}[E]_0$. To analyze the metal ion concentration-dependence of phosphatase activity, the initial rates of phosphatase activity were fitted to Equation 2 to determine values for V_{max} and the apparent Michaelis constant for metal ion dependent-stimulation of enzymatic activity, K_{metal},

$$\nu = V_{\max}[A]/(K_{metal}+[A]), \quad [2]$$

where [*A*] is the concentration of metal ion activator.

Isothermal Titration Calorimetry

ITC measurements were performed using an ITC-200 calorimeter (MicroCal, Northhampton, MA). Titrations were performed in HEPES buffer at 25 °C as specified in the figure legends, with 50 μM and 125 to 175 μM protein for tight and weak metal binding, respectively.

Integrated heats of injection were analyzed using Origin 7.0 software (MicroCal, Northhampton, MA) and were fitted to a one-site binding model or a two independent sites binding model. PP2Cα samples at 10 μM were analyzed for magnesium content by inductively-coupled plasma optical emission spectrometry (ICP-OES) (Intertek, Whitehouse, NJ). The limit of detection of magnesium by this method is below 1 μg/L.

Cell culture, transfection, treatment, protein extraction and immunoblotting

Human HEK293T/clone 17 cells were cultured in Dulbecco's modified Eagle's medium supplemented with 2 mM L-glutamine and 10% fetal bovine serum at 37 °C under a humidified atmosphere containing 5% CO_2. One day after seeding 3×10^6 cells in 10 cm dishes, cells were transfected with 6 μg pWip1-Flag/pCMV-Neo-Bam plasmid DNA mixtures and 12 μL Turbofectin 8.0 (Origene) following the manufacturer's protocol. For WT and mutant Wip1 proteins, the ratios of Wip1-Flag expression plasmid to parental plasmid were as follows: WT, 1:2; D192A, 1:2; D314A, 1:0.6; N318A, 1:0.2. Twenty hours after transfection, cells were exposed to 10 Gy IR in a ^{137}Cs Shepherd Mark II irradiator. After 90 min., the dishes were transferred to ice, and the cells were rinsed with cold PBS, removed by scraping and collected by centrifugation with two additional rinses with cold PBS. Cell pellets were stored at -80 °C. Whole cell lysates were prepared by homogenizing the cell pellet in TNE buffer (10 mM Tris-HCl pH 7.8, 1 mM EDTA, 150 mM NaCl, 1% NP-40, 50 mM NaF) supplemented with protease (Roche) and phosphatase (Sigma) inhibitor cocktails, followed by centrifugation to remove cellular debris. The total protein concentration was determined by the bicinchoninic acid method (Pierce) using BSA as a standard. Protein samples (40 μg) were separated on Nu-PAGE gels (Invitrogen) and transferred onto polyvinylidene difluoride membranes (Millipore). The primary antibodies used were anti-β actin (Sigma), anti-γH2AX (05-636, Millipore), and anti-Wip1 (custom monoclonal M3-311, BD Biosciences). Protein bands were detected using horseradish peroxidase-conjugated secondary antibodies and enhanced chemiluminescence detection (Amersham).

Multiple sequence alignment and positional conservation

Protein sequences were aligned using MUSCLE (37). The alignment of Wip1 and PP2Cα was reported previously (38). Conservation of active site residues (R33, E37, D38, D60, G61, H62, G145, D146, D239, G240, D243, D282) was assessed from the residue frequency tables calculated from the 137 PP2C catalytic domain sequences used to define the Position

Specific Scoring Matrix for identification of the PP2Cc conserved domain from protein sequences (39).

Structural comparison of PP2C active sites

Root mean squared deviations (RSMD) were calculated by comparing the alpha carbon of 11 active site residues of human PP2Cα (PDB 1A6Q) (R33, D38, D60, G61, G145, D146, S147, D239, G240, D282, and N283) to the corresponding atoms in 31 structures. The phosphatase structures with one or two metal ions in the active site (1 or 2M) comprise *H. sapiens* PPM1B (2P8E-A, B), *H. sapiens* PPM1K (4DA1), *B. taurus* Pdp1c (3N3C), *R. norvegicus* Pdp1 (2PNQ-A, B) *A. thaliana* Abi1 (3NMN-B, D), *A. thaliana* Hab1 (3RT0-A, 3RT0-B, 3ZVU-B, 4DS8-B), *M. smegmatis* Mspp (2V06), *M. tuberculosis* PstP (2CM1), *S. agalactiae* SaSTP 2PK0-A, B), and *T. elongates* Tppha-D119A (2Y09). The phosphatase structures with three metal ions in the active site comprise *A. thaliana* Abi2 (3UJK, 3NMV-B, 3UJL-B) *A. thaliana* Hab1 (3QN1-B), *M. smegmatis* Mspp (2JFR, 2JFS), *M .tuberculosis* PstP (1TXO-A, B), *S. agalactiae* SaSTP (2PK0-C, D), *T. elongates* Tppha (2J82). For comparison, RMSDs were also calculated for active site residues of the Rsbu (phosphatase) domain of the *M. tuberculosis* regulatory protein Rv1364c (3KE6-A, B) and the human protein TAB1 (2POM). Significance testing was performed using the 2-tailed Student's T-test with unequal variance.

Results

PP2Cα and Wip1 require supplemental Mg^{2+} for phosphatase activity toward phosphopeptide substrates

PP2Cα and Wip1 are classified as Mg^{2+}- or Mn^{2+}-dependent, phospho-serine or phospho-threonine protein phosphatases. To characterize our preparations of the two enzymes, we determined the substrate- and divalent metal ion-concentration dependence of phosphatase activity. Both proteins were highly active toward the singly-phosphorylated p38α (175-185) (180pT) peptide substrate in the presence of Mg^{2+} ions, minimally active in the presence of Mn^{2+} ions, and inactive in the presence of Ca^{2+} ions or Zn^{2+} ions (Figure 1A), in agreement with previous observations (10, 40). The specificity of the metal ion required to support catalytic activity is affected by the nature of the substrate; both PP2Cα and Wip1 dephosphorylated the chemical substrate pNPP in the presence of Mn^{2+} ions, exhibited minimal activity in the presence of Mg^{2+} ions, and were inhibited by Ca^{2+} or Zn^{2+} ions (data not shown and (10, 40)). For the singly-phosphorylated p38α peptide, both enzymes followed typical saturation kinetics with respect to the substrate and metal ion concentrations (Figure 1B and C). In the presence of 30 mM $MgCl_2$, the K_m values for PP2Cα and Wip1 were 53 and 83 μM, respectively, and the respective k_{cat} values were 4.2 and 2.63 s^{-1}, resulting in a turnover number approximately two-fold greater for PP2Cα than for Wip1. In the presence of 100 μM phosphopeptide, the apparent Michaelis constant, K_{metal}, for Mg^{2+}-dependent activation of catalytic activity was 1.8 mM for PP2Cα and 14 mM for Wip1, similar to values reported previously (10, 40). Interestingly, K_{metal} for Wip1 was about eight-fold higher than for PP2Cα, indicating substantially weaker binding of magnesium ions. Although the requirement for millimolar concentrations of Mg^{2+} or Mn^{2+} for *in vitro* catalytic activity is a defining characteristic of the PP2C phosphatases, its molecular basis, at least for eukaryotic PP2C phosphatases, has not been previously delineated.

Millimolar-affinity binding of magnesium ions to PP2Cα can be detected by isothermal titration calorimetry

To investigate whether millimolar-affinity binding of Mg^{2+} to PP2Cα could be detected directly, we used ITC to measure the heat released or absorbed upon binding. We studied the

tight binding and weak binding of Mg^{2+} to PP2Cα in separate experiments, using different protein and Mg^{2+} ion concentrations for the two affinity ranges. For these experiments, preparations of His tag-free PP2Cα were dialyzed extensively against Chelex resin-treated buffers to remove bound metal ions. As shown in Figure 2A, the titration of PP2Cα with low molar ratios of $MgCl_2$ was exothermic, exhibited relatively modest injection heats, and saturated quickly. For these high-affinity sites, the integrated heats of injection could not be fit to a single-site binding model, consistent with the binding of two metal ions. Although the data could be fit by a two-site model (Figure 2A, lower panel and Table 1), the association constants and enthalpies were not tightly constrained by the data and should be regarded as approximate values. The fitting of complex binding models to ITC data may require performing titrations over an extended range of concentrations of proteins and ligands in order to constrain the values of the fitting parameters (41). For the present purpose, however, these experiments indicate that two Mg^{2+} ions bind to PP2Cα with relatively high (10^5 to 10^6 M^{-1}) but unequal affinities, similar to the characterization of the binding of the two Mn^{2+} ions to PP2Cα based on electron density in the crystal (21). The binding stoichiometries of the two tight-binding sites were highly constrained by the data and are associated with relative uncertainties of less than 20%. Interestingly, the binding stoichiometry of the tighter of the two high-affinity sites (n_1) was approximately 0.4, suggesting that some magnesium remained bound to the apo-PP2Cα even after extensive dialysis against Chelex resin-treated buffers, whereas the fractional occupancy of the weaker of the two high-affinity sites (n_2) was close to 1. To further characterize the apo-PP2Cα preparation, we used ICP-EOS to determine the magnesium content. Analysis of an aliquot of 10 μM apo-PP2Cα indicated a magnesium content of 136 ppb Mg, corresponding to a molar ratio of magnesium to protein of 0.56. Taken together, these results suggest that of the two high-affinity metal binding sites, the higher-affinity site was approximately 60% occupied by Mg^{2+} ions prior to the ITC titration. During the ITC titration, both sites became fully occupied, with binding to the higher-affinity site exhibiting a larger negative enthalpy change and binding to the second site exhibiting a smaller negative enthalpy change.

To detect the millimolar-affinity binding of Mg^{2+} ions to PP2Cα by ITC, we saturated the two high-affinity sites of apo-PP2Cα by adding two equivalents of $MgCl_2$ and performed titrations with higher concentrations of both protein and ligand. The thermogram resulting from titration of PP2Cα·2(Mg^{2+}) with 30 mM $MgCl_2$ is shown in the upper panel of Figure 2B. The process was endothermic and required a large excess of ligand to saturate binding. The integrated heats of injection were well-described by a single-site binding model (Figure 2B, lower panel and Table 1). In contrast to the binding of magnesium ions to the two higher-affinity sites, the binding of the third Mg^{2+} ion to PP2Cα is entropy-driven. The association constant for the binding of a third metal ion to PP2Cα, in the absence of substrate, is $K_a = 0.8 \times 10^3$ M^{-1}. Although the millimolar-affinity binding of a divalent metal ion was anticipated based on the metal ion concentration-dependence of phosphatase activity, this result provides the first thermodynamic characterization of the binding of a metal ion to PP2Cα with millimolar affinity.

Amino acids that coordinate the third metal ion in plant and bacterial PP2C phosphatases are conserved in human PP2Cα and Wip1

To further investigate the binding of a third metal ion to human PP2Cα, we performed a multiple sequence alignment of human PP2Cα with the six structurally-characterized plant and bacterial PP2C phosphatases that display a third Mg^{2+} or Mn^{2+} ion in the active site (Figure 3) (24, 25, 29-31, 33). We annotated the alignment by including designation of the motifs characteristic of the PP2C superfamily (4) and metal-coordinating residues. We also aligned the sequence of Wip1, for which no structural information is available (38, 42). Following the metal ion numbering given previously (21), we refer to the metal ion that is

coordinated by PP2Cα Asp60, Asp239 and Asp282 as M1, and the metal ion that is coordinated by Asp38, Asp60, and Gly61 as M2. Note that in some works, the numbering for these two metal ions is reversed. Two of the residues that coordinate the third metal ion, M3, are highly conserved, as previously noted (24, 30, 31). Specifically, in the structures that display a third metal ion in the active site, residues that align to PP2Cα Asp146 (Wip1 Asp192) coordinate only M3 and residues that align to PP2Cα Asp239 (Wip1 Asp314) coordinate both M1 and M3. Bork and co-workers identified 15 residues that were highly conserved in the PP2C superfamily (4). Twelve of the 15 highly-conserved residues are located in or adjacent to the active site. Six of the highly-conserved residues coordinate a metal ion, including the M3-coordinating dipeptide GlyAsp (PP2Cα 145-146). Of the 15 highly-conserved residues, only the PP2Cα Asp243 position exhibits high variability among the eight proteins. The equivalent residue in Wip1 is Asn318.

In addition to the highly-conserved coordination of M3 by residues aligning to PP2Cα Asp146 and Asp239, some structures feature additional coordination of M3, but the residues involved are highly variable. For the bacterial phosphatases, residues aligning to *M. tuberculosis* PstP Ser160, which is located in the Flap domain, interact with M3, but this interaction is not supported by all structures of a given enzyme. One structure of the *A. thaliana* phosphatase, Hab1, also suggests coordination of the third metal ion by a Flap domain residue, but the location differs from that in the bacterial phosphatases. Furthermore, in several structures, residues aligning to PP2Cα Asp243 are positioned near the third metal ion and may interact through outer-sphere binding or may affect the binding of the third metal ion through indirect mechanisms.

We next examined conservation of the three-dimensional structure of the PP2C active site, including the third-metal coordinating residue Asp146. We compared the positions of the Cα carbons in the active site of the PP2Cα crystal structure to the positions of the corresponding Cα carbons in 11 structures that display three metals in the active site and in 17 structures that display one or two metals in the active site to determine the root mean squared deviations (RMSD) for the active site residues. As shown in Supporting Information Figure S1, the active sites of all 28 structures are very similar to the PP2Cα active site. The average RMSD for active sites with one or two metal ions (0.30 Å) does not differ significantly from the average RMSD for active sites with three metal ions (0.28 Å) ($p = 0.35$). We also calculated RMSDs comparing the active site of PP2Cα to three PP2C-like structures. Although the human TAB1 protein possesses a PP2C-like fold, it does not exhibit phosphatase activity (43). The RsbU domain of the *M. tuberculosis* rv1364c protein is classified as a SpoIIE-like phosphatase, which are distantly related to the PP2C phosphatases (44). The average RMSD for the PP2C-like active sites (0.53 Å) differs significantly from the average RMSD for either PP2C class ($p < 0.005$ for each comparison).

Mutation of putative third metal ion-coordinating amino acids reduces or abolishes millimolar-affinity binding of Mg^{2+} to PP2Cα

The multiple sequence alignment (Figure 3) suggested that Asp146 and Asp239 of PP2Cα are likely to coordinate the third metal ion and that Asp243 may directly or indirectly affect the binding of M3. To test these candidates, we separately mutated to alanine the residues D146, D239 and D243 of PP2Cα and characterized the low-affinity binding of Mg^{2+} to the purified proteins using ITC. For these experiments, His tag-free WT and mutant proteins were purified as before, except that bound metal ions were removed by extensive dialysis against buffer containing EDTA, followed by several changes of buffer without EDTA. Low-affinity ITC experiments were executed as described above, except that the addition of two equivalents of $MgCl_2$ to the apo-protein before the start of the ITC experiment was omitted. As a consequence, the first injection produced a large negative injection heat, which resulted from exothermic binding to the high-affinity sites, whereas subsequent

injections, which produced positive heats, titrated the low-affinity site (Supplementary Figure S2). Disregarding the first injection, the integrated injection heats for the titration of WT, D146A, and D243A PP2Cα proteins with high concentrations of $MgCl_2$ were well described by a single-site model with affinities of the order of 10^3 M^{-1} and positive enthalpies of binding (Table 2). The D146A and D243A mutations each reduced the magnesium binding affinity by about 60%, supporting involvement of each residue in binding a metal ion with millimolar affinity. The finding that PP2Cα D146A still bound a metal ion to the low-affinity site, albeit with reduced affinity, was surprising. Structural studies of active site mutants of the cyanobacterium phosphatase tPphA revealed only two metal ions in the active sites of the D119A (corresponding to human PP2Cα D146) and D193A (corresponding to PP2Cα D239) mutants, whereas wildtype tPphA exhibited three metal ions (28). For PP2Cα D239A protein, the integrated heats of the first two injections were negative and the remainder were not distinguishable from background, suggesting that this mutation abolished the binding of Mg^{2+} to the low-affinity site and reduced binding to high-affinity site(s), in agreement with the expectation that PP2Cα Asp239 coordinates both M1 and M3.

The finding that mutation to alanine of either Asp146 or Asp243 weakened, but did not abolish, Mg^{2+} binding to the low-affinity site suggested that the ion may reside in either of two sub-sites. This notion was supported by variation in the position of the third metal ion among PP2C phosphatase crystal structures (31). To test this hypothesis, we prepared the PP2Cα D146A/D243A double mutant and characterized the binding of Mg^{2+} to the low-affinity site by ITC. For this set of experiments, solutions of WT, D146A and D146A/D243A proteins were supplemented with excess $MgCl_2$ and then dialyzed extensively against buffer containing no $MgCl_2$. Representative thermograms are shown in Figure 4 (top panel). Disregarding the first injection, the integrated injection heats for the WT and D146A PP2Cα proteins were positive and were well described by a single-site model with affinities of the order of 10^3 M^{-1}, with the WT protein exhibiting approximately two-fold tighter binding, similar to the previous experiments. Titration of the double mutant produced only background values of the integrated heats of injection after the first two injections (Figure 4, lower panel and Table 2), demonstrating that the double mutation completely abrogated the millimolar-affinity metal binding. For the WT protein, the integrated heat of the first injection was only slightly higher than that of the second injection, suggesting that occupancy of the two tight-binding sites by Mg^{2+} was only slightly reduced by dialysis against buffer without $MgCl_2$. For the D146A protein, the integrated heat of the first injection was small and negative, suggesting that mutation of Asp146 led to reduced occupancy of the high-affinity sites by Mg^{2+} during dialysis, thus producing a net negative heat for the first injection. For the double mutant, the integrated heat of the first injection was large and negative, suggesting a greater reduction in the occupancy of the high-affinity sites during dialysis. In summary, the ITC experiments characterize the millimolar-affinity binding of Mg^{2+} to PP2Cα as an entropy-driven process that requires Asp239 and that may involve either Asp146 or Asp243.

Substrate- and metal ion-concentration dependence of WT and mutant PP2Cα catalytic activities

To further characterize the role of the third metal ion in catalysis, we measured the steady-state phosphatase activity of the His tag-free WT and active site-mutant PP2Cα proteins using both pNPP and the phosphopeptide as substrates. The phosphopeptide concentration-dependence and $MgCl_2$-concentration dependence of the initial rates were determined as described above and are summarized in Table 3. In addition, phosphatase activity toward the small molecule substrate pNPP was measured in the presence of various concentrations of $MnCl_2$ and was analyzed similarly (Table 3). In agreement with previous observations, WT

PP2Cα exhibited robust phosphatase activity toward the phosphopeptide substrate in the presence of Mg^{2+} and a 75-fold smaller value of the apparent second-order rate constant (k_{cat}/K_m) toward pNPP in the presence of Mn^{2+}. The values of K_{metal} for the two ions are similar. The D146A, D239A and D146A/D243A mutants did not exhibit measurable phosphatase activity toward either substrate under any condition tested. The lack of catalytic activity of D239A was expected because Asp239 is thought to coordinate both M1 and M2. In earlier work, the D239A and D239N mutants were separately reported to be inactive toward phosphoprotein and pNPP substrates, respectively (11, 45). The lack of activity in PP2Cα D146A identifies Asp146 as essential for catalysis, in agreement with previously reported results (28). The lack of catalytic activity in the D146A/D243A mutant follows directly. Compared with the WT enzyme, the activity of D243A toward either substrate was reduced. For both substrates, the presence of high concentrations of metal ions resulted in K_m and k_{cat} values similar to those of the WT enzyme, but the increased values of K_{metal} of the D243A mutant indicate that substitution of alanine for aspartic acid at position 243 weakened the binding of both Mg^{2+} and Mn^{2+}. These results are in accord with the reduced binding affinity of the D243A mutant protein for Mg^{2+} in the absence of substrate, as determined by ITC (Table 2). Interestingly, the value of the apparent second-order rate constant, k_{cat}/K_m, for D243A was 40% that of the WT enzyme for the phosphopeptide substrate in the presence of Mg^{2+}, whereas the value of k_{cat}/K_m for D243A was 76% that of the WT enzyme for activity toward pNPP in the presence of Mn^{2+}. The differential effect of this mutation on activity toward the two substrates suggests that Asp243 may have greater importance in the activity toward phosphopeptide substrates.

Residues in the Flap domain of PP2Cα are important for substrate recognition

Although structural characterization of several PP2C phosphatases have suggested that residues in the Flap domain may provide additional coordination of the third metal ion (24, 25, 29-31), the sequences and structures of the Flap domains exhibit considerable variability among bacterial, plant and human PP2C phosphatases. To further investigate possible roles of the Flap structure in metal binding and catalysis, we generated six mutant proteins with alterations in the Flap region. We tested Arg186 of PP2Cα because our previous work had implicated the corresponding residue of Wip1, Arg243, to be important for substrate recognition (38). PP2Cα Asn188 and Ser190 were tested as residues that potentially provide additional coordination to the third metal ion. His164 and Arg195 are located in the hinge regions on either side of the Flap domain (21, 24). With the phosphopeptide substrate, we observed that the R186A mutant exhibited no activity and the N188A mutant exhibited very low activity, as compared with WT PP2Cα (Table 4). However, both R186A and N188A exhibited substantial activity toward pNPP as a substrate and exhibited a similar Mn^{2+}-dependence of catalytic activity as the WT enzyme (Table 4). These results suggest that both Arg186 and Asn188 are important for phosphopeptide substrate recognition by PP2Cα rather than metal binding. The kinetic parameters of S190A and S190T for both substrates were almost the same as those of WT PP2Cα. Interestingly, Ser190 of PP2Cα aligns near Ser160 of the *M. tuberculosis* phosphatase PstP. Although the crystal structure of PstP indicated coordination of M3 by Ser160, the kinetic constants of the PstP S160A mutant enzyme were similar to WT PstP (24). The PP2Cα hinge-region mutant, R195A, exhibited no activity towards the peptide substrate and reduced activity toward the small molecule pNPP (Table 4). Consistent with these findings, a catalytically-active splice variant of PP2Cα, but not the R195A mutant of the splice variant, inhibited activation of p38 MAPK in cells (9), suggesting that Arg195 is important for PP2Cα activity toward physiological substrates. For the phosphopeptide substrate, the second hinge-region mutant, H164A, exhibited both reduced activity and reduced metal affinity, with K_m and K_{metal} values each almost three times higher than for the WT enzyme; however, the catalytic activity towards pNPP was unaffected (Table 4). Overall, these results indicate that both hinge region

residues affected the catalytic activity of PP2Cα. These results suggest that for PP2Cα, the Flap domain is primarily involved in substrate recognition, but also plays an indirect, substrate-dependent role in metal binding.

The identity of the ion bound to the low-affinity site affects catalytic activity

The above results suggest that several residues in the Flap domain are important for activity toward phosphopeptides in the presence of Mg^{2+} but are not important for activity toward pNPP in the presence of Mn^{2+}. As shown above (Figure 1), the activity of PP2Cα toward phosphopeptide substrates is much higher in the presence of Mg^{2+} than in the presence of Mn^{2+}. To test whether the identities of the metal ions occupying the high-affinity sites or the low-affinity site determined the catalytic activity, we investigated the metal ion concentration-dependence of activity toward the phosphopeptide substrate in the presence of $MgCl_2$, $MnCl_2$, or mixtures of the two salts (Table 5). In the presence of $MgCl_2$ alone, K_{metal} was 1.7 mM and the k_{cat} was 4.6 s^{-1}. Under these conditions, both the high-affinity sites and the low-affinity site were occupied by Mg^{2+}. Addition of 0.1 mM $MnCl_2$ increased the apparent K_{metal} by a factor of 8, but had little effect on k_{cat}. Under these conditions, due to their higher affinity for Mn^{2+}(46), the high-affinity sites were occupied by Mn^{2+} ions and the low-affinity site bound Mg^{2+}. Thus, the presence of the Mg^{2+} ion in the low-affinity site correlated with high catalytic activity toward the phosphopeptide substrate. On the other hand, in the presence of $MnCl_2$ alone, the value of K_{metal} was similar to the value obtained with $MgCl_2$ alone, but the value of k_{cat} was reduced by a factor of 30. Under these conditions, both the high-affinity sites and the low-affinity site were occupied by Mn^{2+}. The presence of the Mn^{2+} ion in the low-affinity site correlated with low catalytic activity toward the phosphopeptide substrate. The results of varying the concentration of $MnCl_2$ in the presence of 0.1 mM $MgCl_2$ did not differ from those with $MnCl_2$, a result consistent with the much higher affinity of Mn^{2+} than Mg^{2+} for the tight sites.

The apparent metal affinity of PP2Cα is reduced at low pH

In the reported crystal structure of PP2Cα, only two bound metal ions were observed (21). It has been suggested that the acidic pH of the crystallization conditions may have reduced the affinity for binding the third metal ion (24, 29, 31). To evaluate the effect of pH on metal binding to PP2Cα, we determined the metal ion-concentration dependence of catalytic activity toward a phosphopeptide substrate at three different pH values (Figure 5). The results show increased catalytic activity with increasing pH over this range, in agreement with earlier results characterizing the pH-dependence of activity toward pNPP in the presence of Mn^{2+}(22). The log of the catalytic constant, k_{cat}, increased linearly with increasing pH with a slope of 0.68 (Figure 5B, left axis), in agreement with the suggestion from a different analysis that an ionizable group with a neutral pK_a must be unprotonated for catalysis (22). Similarly, the log of the inverse of K_{metal} increased linearly with increasing pH with a slope of 0.54 (Figure 5B, right axis), suggesting that a net release of half of a proton accompanies metal ion binding. These results suggest that the binding of a catalytically necessary metal ion, with approximately millimolar affinity, contributes substantially to the observed pH-dependence of PP2Cα catalytic activity.

Mutation of putative third metal ion-coordinating residues of Wip1 reduces or abrogates catalytic activity in vitro and in vivo

As shown above (Figure 3), the residues that have been shown to directly or indirectly coordinate a third active site metal ion in structurally-characterized PP2C phosphatases are conserved in PP2Cα and Wip1. To examine the importance of the third metal for the phosphatase activity of Wip1, we generated alanine mutants of the corresponding metal-coordinating residues and measured the metal ion-concentration dependence of the catalytic activity using the phosphopeptide substrate. As Asp314 of Wip1, corresponding to Asp239

of PP2Cα, has similarly been reported to be catalytically inactive (8), we did not further characterize its phosphatase activity in vitro. Similar to the D146A mutant of PP2Cα, the D192A mutant was completely inactive (Figure 6A), suggesting an essential role of Wip1 Asp192 in catalysis. The apparent metal affinity of Wip1 N318A (19 mM) was only 30% weaker than that of WT Wip1 (14 mM), in contrast to the three-fold reduction in the apparent metal affinity of the corresponding PP2Cα D243A mutant compared with WT PP2Cα. Interestingly, however, the apparent k_{cat} of Wip1 N318A (0.84 s^{-1}) was approximately three-fold lower than that of WT Wip1 (2.23 s^{-1}), whereas the apparent k_{cat} of PP2Cα D243A was almost the same as that of WT PP2Cα. Thus, both Wip1 N318A and PP2Cα D243A exhibit substantially reduced phosphatase activity.

To investigate whether mutation of these residues affected phosphatase activity in mammalian cells, we over-expressed WT or mutant Wip1 proteins in HEK293T cells and determined the level of phosphorylation of H2AX following exposure to IR (Figure 6B). The formation of γH2AX by phosphorylation of Ser139 of the histone H2 variant H2AX is important in damage response signaling and for the assembly of DNA repair complexes (19, 47). γH2AX has been identified as a target of Wip1 phosphatase activity (14-16). As shown in Figure 6B, overexpression of WT Wip1-Flag in HEK 293T cells, when examined 90 min after exposure to IR, resulted in a dramatically reduced level of γH2AX, compared with cells transiently-transfected with the parental vector, in agreement with previous results (14, 16). Interestingly, in cells overexpressing either Wip1 D192A-Flag or Wip1-D314A-Flag, despite a higher level of the mutant protein compared with WT protein, the γH2AX level was similar to that detected in cells transfected with the parental vector, suggesting minimal phosphatase activity. Furthermore, overexpression of Wip1-N318A-Flag resulted in a level of γH2AX similar to that in cells transfected with WT Wip1-Flag, despite a much higher level of Wip1-N318A-Flag protein compared with WT Wip1- Flag protein. This result suggests that the phosphatase activity of the Wip1-N318A protein is markedly reduced compared to that of the WT protein. Thus the in vitro and in vivo phosphatase activities of the mutant Wip1 proteins conform to the same pattern. Phosphatase activity is abolished by the mutation to alanine of either Asp192, which is expected to coordinate M3, or Asp314, which is expected to coordinate M1 and M3. Mutation to alanine of the peripheral residue Asn318 resulted in reduced activity in both in vitro and in vivo assays.

Third metal ion-coordinating residues are conserved in most PP2C phosphatases

As mentioned above, the putative M3-coordinating amino acid Asp146 of PP2Cα is one of the 15 highly-conserved residues identified by Bork *et al.* (see Figure 3 and (4)). As a further comparison, we performed a multiple sequence alignment of the catalytic domains of 18 human PP2C domain-containing proteins and examined the conservation of active site residues (Supporting Information Figure S3). In the alignment, integrin-linked kinase-associated serine/threonine phosphatase (ILKAP) and the 12 PPM1 proteins cluster together and exhibit high conservation of the active site residues, including the conservation of the aspartic acid residue aligning to PP2Cα Asp146. Pyruvate dehyrogenase phosphatase 1 (PDP1) and PDP2 differ from the PPM1 proteins in motif 1 (PP2Cα D38) and motif 11 (PP2Cα D282), but remain highly similar in motif 2 (PP2Cα D60), motif 5 (PP2Cα D146), and motif 8 (PP2Cα D239). PH domain and leucine rich repeat protein phosphatase 1 (PHLPP1) and PHLPP2, which share sequence homology with both the leucine-rich repeat and PP2C portions of yeast adenylate cyclases, specifically dephosphorylate hydrophobic-motif phosphoserines that regulate the activity of specific kinases (48, 49). For PHLPP1 and PHLPP2, the residues that align to PP2Cα Asp146 are lysine and threonine, respectively. The human TAB1 protein has a fold that closely resembles the PP2C fold, but binds only one metal ion and does not exhibit phosphatase activity (43). In summary, the 12 PPM1

phosphatases as well as ILKAP, PDP1 and PDP2, all retain aspartic acid as the residue aligning to PP2Cα Asp146.

The PP2C active site is highly conserved and is usually identified as residues aligning to the eight PP2Cα residues: aa 33, 37-38, 60-62, 239 and 282, corresponding to the residues that coordinate the phosphate, coordinate the two metal ions, or serve as a proton donor (21). We examined the conservation of these eight residues, along with the putative M3-binding residue Asp146, its neighboring residues Gly145 and Ser147, as well as Gly240, Asp243, and Asn283, among a set of PP2C catalytic domain sequences. As shown in Supporting Information Figure S4, the putative M3-coordinating residues (aa 146, 239) are as highly conserved as the M1-coordinating residues (aa 60, 239, 282) and the M2-coordinating residues (aa 38, 60, 61).

Discussion

From the PP2Cα crystal structure and analysis of reaction kinetics, it was previously thought that only two metals were bound in the active center of human PP2Cα (21). The proposed catalytic mechanism in human PP2Cα was an SN2 reaction controlled by the two metal ions and coordinated water molecules (21, 22). Still, the two Mn^{2+} ions visualized in the crystal structure were bound with at least micromolar affinities and thus did not explain the millimolar concentrations of Mn^{2+} or Mg^{2+} required for *in vitro* phosphatase activity. Recently, crystal structures of several bacterial and plant PP2C phosphatases have shown the presence of three metal ions in the active site (24, 25, 28-31). In the cyanobacterium phosphatase tPphA, mutation to alanine of Asp119, which corresponds to PP2Cα Asp146, resulted in loss of catalytic activity (28). The high degree of conservation of the third metal ion-coordinating residues implied that human PP2C phosphatases may also bind a third metal ion (24, 25, 28). In this study, we have demonstrated that at least three metal ions are bound by PP2Cα, with the third ion having an affinity in the millimolar range. This weak binding was reduced by mutation to alanine of Asp146 or Asp243 and was abolished by mutation to alanine of Asp239 or the combination of Asp146 and Asp243. In addition, our findings suggest that the binding of the third metal ion is necessary for PP2Cα catalytic activity, as both the D146A and D239A mutants were catalytically inactive and the D243A mutant showed reduced activity. On the basis of these results, we propose the presence of a catalytically-required, third metal ion-binding site in PP2Cα that is composed of at least Asp146 and Asp239 and is affected by the presence of Asp243. Moreover, mutation of the corresponding residues in Wip1 similarly affected phosphatase activity both in vitro and in human cells, suggesting that Wip1 catalytic activity similarly requires the binding of a third metal ion. Interestingly, mutation to alanine of Asp243 of PP2Cα reduced the apparent magnesium ion affinity by a factor of three without affecting k_{cat}, whereas mutation to alanine of Asn318 of Wip1 reduced both k_{cat} and the apparent affinity of magnesium ion binding.

Extensive kinetic analysis of PP2Cα demonstrated that enzymatic catalysis proceeds via an ordered sequential mechanism in which the metal ion binds to the enzyme before binding of the substrate (pNPP) and is released after the release of the products (22). This mechanism suggests that the binding of a catalytically-significant metal ion may increase the affinity of the substrate for the enzyme, an anticipated role of Mg^{2+} ions in metallohydrolase catalytic activity (50). An additional possibility, more specifically for phosphopeptide substrates, is that the substrate itself may bind metal ions (51).

Several mammalian PP2C phosphatases, including PP2Cα, Wip1 and PPM1H, exhibit metal-dependent substrate preferences, in that the enzymes exhibit more stringent specificity toward phosphoprotein or selected phosphopeptide substrates in the presence of Mg^{2+} and

exhibit reduced specificity, including activity toward pNPP, in the presence of Mn^{2+} (10, 40, 52). Although frequently used to demonstrate activity of protein serine/threonine phosphatases, pNPP has been termed a “bulky” substrate because the presence of a phenyl ring makes it a more suitable model substrate for tyrosine phosphatases (52). In the presence of Mg^{2+}, both PP2Cα and Wip1 exhibit high k_{cat}/K_m values for suitable phosphopeptide substrates and low values for pNPP (this work and (10, 40)), suggesting that the magnesium-based specificity more closely reflects protein serine/threonine phosphatase characteristics. Interestingly, our results demonstrate that the identity of the metal bound to the low-affinity site is particularly crucial for this substrate specificity, as the presence of Mg^{2+}, rather than Mn^{2+}, bound to the low-affinity site correlated with high activity toward phosphopeptide substrates.

Our detection of the binding of a third Mg^{2+} ion to PP2Cα by ITC required a high molar ratio of $MgCl_2$ to protein to saturate the site. In a recent study using ITC, the binding of Mn^{2+} to the *T. elongatus* phosphatase, tPphA, provided evidence for the binding of three metal ions, whereas a similar experiment characterizing the binding of Mn^{2+} to human PP2Cα suggested that only two ions are bound (28). Our ITC results for magnesium binding to human PP2Cα (Figure 2) suggest that the $MnCl_2$ concentrations in their experiments may have been too low to detect the binding of the third metal ion. It should also be noted that the PP2Cα crystal was grown in the presence of 2 mM $MnCl_2$(21), whereas the crystallization buffers for bacterial PP2C phosphatase structures that displayed three metal ions in the active site included markedly higher concentrations of metal ions (24, 25, 28-31).

Another possible reason that the PP2Cα crystal structure included only two metal ions was that the crystallization buffer had a pH of 5.0 (21). It has been noted previously that the activity of PP2Cα is very low under this condition and that the structure may correspond to an inactive form of the enzyme (22). Our results showed that lower pH values reduced the apparent metal affinity as well as the activity of PP2Cα. The possibility that the low pH of the crystallization buffer may have led to a loss of metal coordination in human PP2Cα was also suggested in a report on the MspP crystal structure (31). For this bacterial phosphatase, crystals that were grown at pH 8.5 included three metal ions in the active site, whereas crystals grown at pH 5.5 contained only two metal ions. The loss of PP2Cα activity at pH 5.0 has been suggested to result from incorrect protonation (22). Our results suggest that the loss of M3 coordination at low pH also contributes to the reduction in activity at low pH.

Interactions between adjacent monomers in the crystal may have further contributed to the absence of a third metal ion in the PP2Cα structure. The binding site of the third ion, located at one end of the catalytic groove, is a point of contact between monomers in the crystal. As depicted in Supporting Information Figure S4, the side chain of Lys303 from an adjacent monomer protrudes into the active site, forming a salt bridge with the potentially M3-coordinating residue Asp243 and potentially affecting the conformation of the M1/M3-coordinating residue Asp239. These perturbations may have resulted in a reduced affinity for the third ion. Furthermore, the adjacent monomer also interacts with the Flap domain (Figure S5), potentially altering its conformation.

It has been suggested that translocation of the Flap domain during turnover may affect metal binding and substrate recognition (24). Several of our findings support this hypothesis, including the reduced affinity of the PP2Cα H164A mutant for Mg^{2+} measured in the presence of the peptide substrate, the loss of activity of the PP2Cα R195A mutant, and the specific substrate recognition patterns of the PP2Cα R186A and N188A mutants. Consistent with this, the catalytic efficiency of tPphA R169A (equivalent to PP2Cα R195A) was 30% that of the WT enzyme (25). Furthermore, mutation to alanine of Wip1 Arg243 (equivalent to PP2Cα Arg186) resulted in loss of activity toward a peptide substrate (38). In the crystal

structure of SaSTP, contacts among the four monomers in the unit cell have been interpreted as resembling two pairs of enzyme-substrate complexes (30). Interestingly, in each pair, the SaSTP monomer taking the role of “enzyme” contains three metal ions in the active site and has an altered conformation of the Flap domain that interacts with the “substrate” monomer. In addition, the Flap domain of the *A. thaliana* PP2C phosphatase Hab1 is the main interface for intermolecular contacts with a member of the Pyr/Pyl/Rcar plant hormone receptor family (33). Thus, evidence supporting the involvement of the Flap domain in substrate recognition has been accumulating.

The PP2C phosphatases are characterized by their requirement for supplementation with Mg^{2+} or Mn^{2+} ions to exhibit phosphatase activity in vitro. Experiments with purified enzymes are typically performed in the presence of 10 to 30 mM $MgCl_2$ or $MnCl_2$. The K_{metal} values we determined for PP2Cα and Wip1, using a phosphopeptide as the substrate, were 1.8 mM and 14 mM, respectively, and the dissociation constant determined by ITC for the binding of Mg^{2+} to PP2Cα in the absence of substrate was similar to the value of K_{metal} determined from kinetic assays. In mammalian cells, most magnesium ions are bound to nucleotides, nucleic acids and proteins, and the concentration of free Mg^{2+} ranges from 0.4 to 1 mM (53). For PP2Cα, if the binding constant determined in vitro also applies in vivo, the kinetically-necessary magnesium binding site would be only partially occupied and the enzyme would not be fully active. However, this state of partial activation may reflect physiological regulation of the enzyme activity. For example, PP2Cα has been shown to increase insulin sensitivity by activating PI3K (54). Insulin itself increases the intracellular concentration of free Mg^{2+} ions (55), providing a potential mechanism for activation of PP2Cα. Insulin also increases the affinity of PDP1 for Mg^{2+}, stimulating its phosphatase activity (56) and thereby increasing the activity of the mitochondrial pyruvate dehydrogenase complex. Interestingly, PDP1 from obese subjects is less active and has reduced affinity for Mg^{2+} (57).

In cells, PP2C phosphatases may be activated by endogenous cellular components or specific signaling molecules that increase the enzyme's affinity for magnesium or manganese ions. PP2Cα has been reported to be activated by fatty acids in the presence of physiological concentrations of Mg^{2+} ions (58). In addition, PPM1G and PP2Cα are activated by ceramides (59). For Wip1, which displays eight-fold weaker binding to magnesium than PP2Cα, the possible involvement of activating molecules in cells becomes more compelling.

The requirement for supplementation with millimolar concentrations of Mg^{2+} or Mn^{2+} is a defining characteristic of the PP2C phosphatases that has remained enigmatic while the mechanism was restricted to the involvement of a bi-metal catalytic center. Recent structural studies of some bacterial and plant PP2C phosphatases have revealed the presence of a third metal ion in the active site and have suggested that its involvement in the catalytic mechanism was likely to be a general characteristic of the PP2C phosphatases. Our results provide a thermodynamic and kinetic characterization of a third Mg^{2+} ion binding to human PP2Cα and show that the aligned residues of human Wip1 are similarly involved. Our findings, together with other recent reports, suggest that the third metal ion plays complex roles in catalysis and the determination of substrate specificity that remain incompletely understood. Further investigation of the catalytic mechanism, including the role of the Flap domain, will help in understanding the physiological functions of the PP2C phosphatases and the development of specific inhibitors and activators.

Supplementary Material

Refer to Web version on PubMed Central for supplementary material.

Acknowledgments

We thank William K. Gillette (Protein Expression Laboratory, NCI-Frederick) for helpful discussions on protein purification.

This research was supported by the Intramural Research Program of the Center for Center Research, National Cancer Institute, National Institutes of Health.

References

1. Lammers T, Lavi S. Role of type 2C protein phosphatases in growth regulation and in cellular stress signaling. Crit Rev Biochem Mol Biol. 2007; 42:437–461. [PubMed: 18066953]
2. Moorhead GB, De Wever V, Templeton G, Kerk D. Evolution of protein phosphatases in plants and animals. Biochem J. 2009; 417:401–409. [PubMed: 19099538]
3. Shi Y. Serine/threonine phosphatases: mechanism through structure. Cell. 2009; 139:468–484. [PubMed: 19879837]
4. Bork P, Brown NP, Hegyi H, Schultz J. The protein phosphatase 2C (PP2C) superfamily: detection of bacterial homologues. Protein Sci. 1996; 5:1421–1425. [PubMed: 8819174]
5. Brognard J, Sierecki E, Gao T, Newton AC. PHLPP and a second isoform, PHLPP2, differentially attenuate the amplitude of Akt signaling by regulating distinct Akt isoforms. Mol Cell. 2007; 25:917–931. [PubMed: 17386267]
6. Peng A, Maller JL. Serine/threonine phosphatases in the DNA damage response and cancer. Oncogene. 2010; 29:5977–5988. [PubMed: 20838380]
7. Fiscella M, Zhang H, Fan S, Sakaguchi K, Shen S, Mercer WE, Vande Woude GF, O'Connor PM, Appella E. Wip1, a novel human protein phosphatase that is induced in response to ionizing radiation in a p53-dependent manner. Proc Natl Acad Sci U S A. 1997; 94:6048–6053. [PubMed: 9177166]
8. Takekawa M, Adachi M, Nakahata A, Nakayama I, Itoh F, Tsukuda H, Taya Y, Imai K. p53-inducible wip1 phosphatase mediates a negative feedback regulation of p38 MAPK-p53 signaling in response to UV radiation. EMBO J. 2000; 19:6517–6526. [PubMed: 11101524]
9. Takekawa M, Maeda T, Saito H. Protein phosphatase 2Calpha inhibits the human stress-responsive p38 and JNK MAPK pathways. EMBO J. 1998; 17:4744–4752. [PubMed: 9707433]
10. Yamaguchi H, Minopoli G, Demidov ON, Chatterjee DK, Anderson CW, Durell SR, Appella E. Substrate specificity of the human protein phosphatase 2Cdelta, Wip1. Biochemistry. 2005; 44:5285–5294. [PubMed: 15807522]
11. Ofek P, Ben-Meir D, Kariv-Inbal Z, Oren M, Lavi S. Cell Cycle regulation and p53 activation by protein phosphatase 2C alpha. J Biol Chem. 2003; 278:14299–14305. [PubMed: 12514180]
12. Lu X, Nannenga B, Donehower LA. PPM1D dephosphorylates Chk1 and p53 and abrogates cell cycle checkpoints. Genes & Dev. 2005; 19:1162–1174. [PubMed: 15870257]
13. Shreeram S, Demidov ON, Hee WK, Yamaguchi H, Onishi N, Kek C, Timofeev ON, Dudgeon C, Fornace AJ, Anderson CW, Minami Y, Appella E, Bulavin DV. Wip1 phosphatase modulates ATM-dependent signaling pathways. Mol Cell. 2006; 23:757–764. [PubMed: 16949371]
14. Cha H, Lowe JM, Li H, Lee JS, Belova GI, Bulavin DV, Fornace AJ Jr. Wip1 directly dephosphorylates gamma-H2AX and attenuates the DNA damage response. Cancer Res. 2010; 70:4112–4122. [PubMed: 20460517]
15. Macurek L, Lindqvist A, Voets O, Kool J, Vos HR, Medema RH. Wip1 phosphatase is associated with chromatin and dephosphorylates gammaH2AX to promote checkpoint inhibition. Oncogene. 2010; 29:2281–2291. [PubMed: 20101220]
16. Moon SH, Lin L, Zhang X, Nguyen TA, Darlington Y, Waldman AS, Lu X, Donehower LA. Wild-type p53-induced phosphatase 1 dephosphorylates histone variant gamma-H2AX and suppresses DNA double strand break repair. J Biol Chem. 2010; 285:12935–12947. [PubMed: 20118229]
17. Lu X, Ma O, Nguyen TA, Jones SN, Oren M, Donehower LA. The Wip1 Phosphatase acts as a gatekeeper in the p53-Mdm2 autoregulatory loop. Cancer Cell. 2007; 12:342–354. [PubMed: 17936559]

18. Le Guezennec X, Bulavin DV. WIP1 phosphatase at the crossroads of cancer and aging. Trends Biochem Sci. 2012; 35:109–114. [PubMed: 19879149]
19. Lowe J, Cha H, Lee MO, Mazur SJ, Appella E, Fornace AJ Jr. Regulation of the Wip1 phosphatase and its effects on the stress response. Front Biosci. 2012; 17:1480–1498.
20. Lu X, Nguyen TA, Moon SH, Darlington Y, Sommer M, Donehower LA. The type 2C phosphatase Wip1: an oncogenic regulator of tumor suppressor and DNA damage response pathways. Cancer Metastasis Rev. 2008; 27:123–135. [PubMed: 18265945]
21. Das AK, Helps NR, Cohen PT, Barford D. Crystal structure of the protein serine/threonine phosphatase 2C at 2.0 A resolution. EMBO J. 1996; 15:6798–6809. [PubMed: 9003755]
22. Fjeld CC, Denu JM. Kinetic analysis of human serine/threonine protein phosphatase 2Calpha. J Biol Chem. 1999; 274:20336–20343. [PubMed: 10400656]
23. Mitic N, Smith SJ, Neves A, Guddat LW, Gahan LR, Schenk G. The catalytic mechanisms of binuclear metallohydrolases. Chem Rev. 2006; 106:3338–3363. [PubMed: 16895331]
24. Pullen KE, Ng HL, Sung PY, Good MC, Smith SM, Alber T. An alternate conformation and a third metal in PstP/Ppp, the M. tuberculosis PP2C-Family Ser/Thr protein phosphatase. Structure. 2004; 12:1947–1954. [PubMed: 15530359]
25. Schlicker C, Fokina O, Kloft N, Grune T, Becker S, Sheldrick GM, Forchhammer K. Structural analysis of the PP2C phosphatase tPphA from Thermosynechococcus elongatus: a flexible flap subdomain controls access to the catalytic site. J Mol Biol. 2008; 376:570–581. [PubMed: 18164312]
26. Kennelly PJ. Protein phosphatases--a phylogenetic perspective. Chem Rev. 2001; 101:2291–2312. [PubMed: 11749374]
27. Su J, Forchhammer K. Determinants for substrate specificity of the bacteria PP2C protein phosphatase tPphA from Thermosynechococcus elongatus. The FEBS J. 2012
28. Su J, Schlicker C, Forchhammer K. A third metal is required for catalytic activity of the signal-transducing protein phosphatase M tPphA. J Biol Chem. 2011; 286:13481–13488. [PubMed: 21310952]
29. Bellinzoni M, Wehenkel A, Shepard W, Alzari PM. Insights into the catalytic mechanism of PPM Ser/Thr phosphatases from the atomic resolution structures of a mycobacterial enzyme. Structure. 2007; 15:863–872. [PubMed: 17637345]
30. Rantanen MK, Lehtio L, Rajagopal L, Rubens CE, Goldman A. Structure of Streptococcus agalactiae serine/threonine phosphatase. The subdomain conformation is coupled to the binding of a third metal ion. EMBO J. 2007; 274:3128–3137.
31. Wehenkel A, Bellinzoni M, Schaeffer F, Villarino A, Alzari PM. Structural and binding studies of the three-metal center in two mycobacterial PPM Ser/Thr protein phosphatases. J Mol Biol. 2007; 374:890–898. [PubMed: 17961594]
32. Dupeux F, Antoni R, Betz K, Santiago J, Gonzalez-Guzman M, Rodriguez L, Rubio S, Park SY, Cutler SR, Rodriguez PL, Marquez JA. Modulation of abscisic acid signaling in vivo by an engineered receptor-insensitive protein phosphatase type 2C allele. Plant Physiol. 2011; 156:106–116. [PubMed: 21357183]
33. Melcher K, Ng LM, Zhou XE, Soon FF, Xu Y, Suino-Powell KM, Park SY, Weiner JJ, Fujii H, Chinnusamy V, Kovach A, Li J, Wang Y, Li J, Peterson FC, Jensen DR, Yong EL, Volkman BF, Cutler SR, Zhu JK, Xu HE. A gate-latch-lock mechanism for hormone signalling by abscisic acid receptors. Nature. 2009; 462:602–608. [PubMed: 19898420]
34. Soon FF, Ng LM, Zhou XE, West GM, Kovach A, Tan MH, Suino-Powell KM, He Y, Xu Y, Chalmers MJ, Brunzelle JS, Zhang H, Yang H, Jiang H, Li J, Yong EL, Cutler S, Zhu JK, Griffin PR, Melcher K, Xu HE. Molecular mimicry regulates ABA signaling by SnRK2 kinases and PP2C phosphatases. Science. 2012; 335:85–88. [PubMed: 22116026]
35. Moon SH, Nguyen TA, Darlington Y, Lu X, Donehower LA. Dephosphorylation of gamma-H2AX by WIP1: an important homeostatic regulatory event in DNA repair and cell cycle control. Cell Cycle. 2010; 9:2092–2096. [PubMed: 20495376]
36. Baker SJ, Markowitz S, Fearon ER, Willson JK, Vogelstein B. Suppression of human colorectal carcinoma cell growth by wild-type p53. Science. 1990; 249:912–915. [PubMed: 2144057]

37. Edgar RC. MUSCLE: a multiple sequence alignment method with reduced time and space complexity. BMC Bioinform. 2004; 5:113.
38. Hayashi R, Tanoue K, Durell SR, Chatterjee DK, Jenkins LM, Appella DH, Appella E. Optimization of a cyclic peptide inhibitor of Ser/Thr phosphatase PPM1D (Wip1). Biochemistry. 2011; 50:4537–4549. [PubMed: 21528848]
39. Marchler-Bauer A, Zheng C, Chitsaz F, Derbyshire MK, Geer LY, Geer RC, Gonzales NR, Gwadz M, Hurwitz DI, Lanczycki CJ, Lu F, Lu S, Marchler GH, Song JS, Thanki N, Yamashita RA, Zhang D, Bryant SH. CDD: conserved domains and protein three-dimensional structure. Nucl Acids Res. 2013; 41:D348–352. [PubMed: 23197659]
40. Marley AE, Sullivan JE, Carling D, Abbott WM, Smith GJ, Taylor IW, Carey F, Beri RK. Biochemical characterization and deletion analysis of recombinant human protein phosphatase 2C alpha. Biochem J. 1996; 320(3):801–806. [PubMed: 9003365]
41. Houtman JC, Brown PH, Bowden B, Yamaguchi H, Appella E, Samelson LE, Schuck P. Studying multisite binary and ternary protein interactions by global analysis of isothermal titration calorimetry data in SEDPHAT: application to adaptor protein complexes in cell signaling. Protein Sci. 2007; 16:30–42. [PubMed: 17192587]
42. Chuman Y, Yagi H, Fukuda T, Nomura T, Matsukizono M, Shimohigashi Y, Sakaguchi K. Characterization of the active site and a unique uncompetitive inhibitor of the PPM1-type protein phosphatase PPM1D. Protein Peptide Lett. 2008; 15:938–948.
43. Conner SH, Kular G, Peggie M, Shepherd S, Schuttelkopf AW, Cohen P, Van Aalten DM. TAK1-binding protein 1 is a pseudophosphatase. Biochem J. 2006; 399:427–434. [PubMed: 16879102]
44. King-Scott J, Konarev PV, Panjikar S, Jordanova R, Svergun DI, Tucker PA. Structural characterization of the multidomain regulatory protein Rv1364c from Mycobacterium tuberculosis. Structure. 2011; 19:56–69. [PubMed: 21220116]
45. Jackson MD, Fjeld CC, Denu JM. Probing the function of conserved residues in the serine/threonine phosphatase PP2Calpha. Biochemistry. 2003; 42:8513–8521. [PubMed: 12859198]
46. Wynn RM, Li J, Brautigam CA, Chuang JL, Chuang DT. Structural and biochemical characterization of human mitochondrial branched-chain alpha-ketoacid dehydrogenase phosphatase. J Biol Chem. 287:9178–9192. [PubMed: 22291014]
47. Bonner WM, Redon CE, Dickey JS, Nakamura AJ, Sedelnikova OA, Solier S, Pommier Y. GammaH2AX and cancer. Nature Rev. 2008; 8:957–967.
48. Shimizu K, Okada M, Takano A, Nagai K. SCOP, a novel gene product expressed in a circadian manner in rat suprachiasmatic nucleus. FEBS Lett. 1999; 458:363–369. [PubMed: 10570941]
49. Gao T, Furnari F, Newton AC. PHLPP: a phosphatase that directly dephosphorylates Akt, promotes apoptosis, and suppresses tumor growth. Mol Cell. 2005; 18:13–24. [PubMed: 15808505]
50. Klotz IM, Loh Ming wC. Mediation by Metals of the Binding of Small Molecules by Proteins. J Amer Chem Soc. 1954; 76:805–814.
51. Liu S, Zhang C, Campbell JL, Zhang H, Yeung KK, Han VK, Lajoie GA. Formation of phosphopeptide-metal ion complexes in liquid chromatography/electrospray mass spectrometry and their influence on phosphopeptide detection. Rapid Commun Mass Spectrom. 2005; 19:2747–2756. [PubMed: 16136520]
52. Sugiura T, Noguchi Y. Substrate-dependent metal preference of PPM1H, a cancer-associated protein phosphatase 2C: comparison with other family members. Biometals. 2009; 22:469–477. [PubMed: 19262998]
53. Krieglstein J, Selke D, Maassen A, Klumpp S. Activity of PP2C beta is increased by divalent cations and lipophilic compounds depending on the substrate. Meth Enzymol. 2003; 366:282–289. [PubMed: 14674255]
54. Yoshizaki T, Maegawa H, Egawa K, Ugi S, Nishio Y, Imamura T, Kobayashi T, Tamura S, Olefsky JM, Kashiwagi A. Protein phosphatase-2C alpha as a positive regulator of insulin sensitivity through direct activation of phosphatidylinositol 3-kinase in 3T3-L1 adipocytes. J Biol Chem. 2004; 279:22715–22726. [PubMed: 15016818]

55. Delva P, Degan M, Trettene M, Lechi A. Insulin and glucose mediate opposite intracellular ionized magnesium variations in human lymphocytes. J Endocrinol. 2006; 190:711–718. [PubMed: 17003272]

56. Thomas AP, Diggle TA, Denton RM. Sensitivity of pyruvate dehydrogenase phosphate phosphatase to magnesium ions. Similar effects of spermine and insulin. Biochem J. 1986; 238:83–91. [PubMed: 3026347]

57. Piccinini M, Mostert M, Alberto G, Ramondetti C, Novi RF, Dalmasso P, Rinaudo MT. Down-regulation of pyruvate dehydrogenase phosphatase in obese subjects is a defect that signals insulin resistance. Obesity Res. 2005; 13:678–686.

58. Klumpp S, Selke D, Hermesmeier J. Protein phosphatase type 2C active at physiological Mg2+: stimulation by unsaturated fatty acids. FEBS Lett. 1998; 437:229–232. [PubMed: 9824296]

59. Perry DM, Kitatani K, Roddy P, El-Osta M, Hannun YA. Identification and characterization of protein phosphatase 2C activation by ceramide. J Lipid Res. 2012; 53:1513–1521. [PubMed: 22615346]

Abbreviations

ATM	Ataxia telangiectasia mutated
EDTA	Ethylenediaminetetraacetic acid
EGTA	ethylene glycol tetraacetic acid
HEPES	4-2-Hydroxyethyl-1-piperazineethanesulfonic acid
ILKAP	integrin-linked kinase-associated serine/threonine phosphatase
IPTG	Isopropyl β-D-1-thiogalactopyranoside
ICP-OES	Inductively-coupled plasma optical emission spectrometry
IR	ionizing radiation
ITC	Isothermal Titration Calorimetry
LB	Luria-Bertani broth
MAPK p38α	mitogen-activated protein kinase 1
MES	2-(N-morpholino)ethanesulfonic acid
p53	Tumor Protein p53 (TP53)
PBS	phosphate-buffered saline
PDB	Protein Data Bank
PDP	Pyruvate Dehydrogenase Phosphatase
PHLPP	PH domain and leucine rich repeat protein phosphatase
PP2Cα	PPM1A
PPM1A	protein phosphatase, Mg^{2+}/Mn^{2+} dependent, 1A (PP2Cα)
PPM1D	protein phosphatase, Mg^{2+}/Mn^{2+} dependent, 1D (Wip1)
TEV	Tobacco Etch Virus
Tris	tris(hydroxymethyl)aminomethane
Wip1	PPM1D
WT	wildtype
β-ME	2-Mercaptoethanol

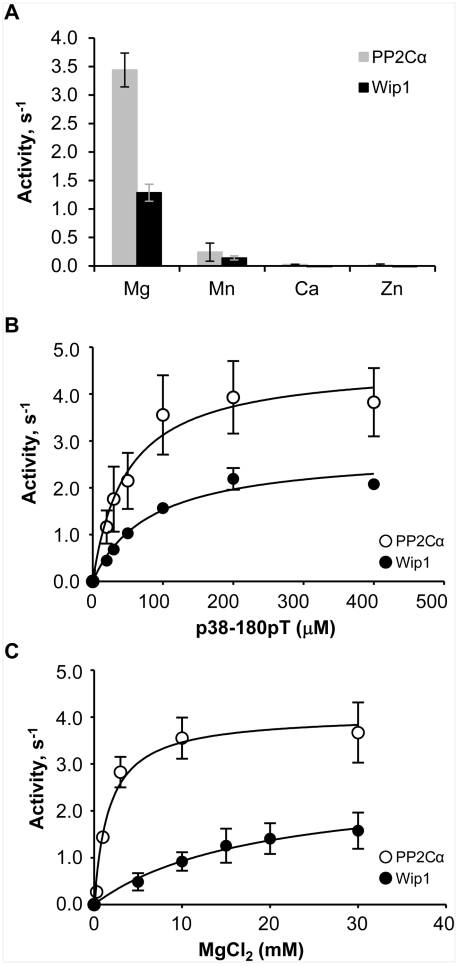

Figure 1.

Substrate- and metal ion dependence of steady state phosphatase activity of human PP2Cα and Wip1. Activity assays were performed at 30 °C and contained 15 ng purified PP2Cα or 60 ng purified ProS2-Wip1(1-420). The initial rates were fitted to the Michaelis-Menten equation. Each point represents the average of at least three independent measurements. (A) Metal ion dependence of phosphatase activity. The activity was measured with 100 μM p38α(175-185)(180pT) peptide in the presence of 30 mM of the indicated chloride salts. (B) Phosphopeptide concentration dependence of phosphatase activity. The activity was measured with 0-400 μM p38α(175-185)(180pT) peptide in the presence of 30 mM $MgCl_2$. (C) $MgCl_2$ concentration dependence of phosphatase activity. The activity was measured with 0.3-30 mM $MgCl_2$ in the presence of 100 μM p38α(175-185)(180pT) peptide.

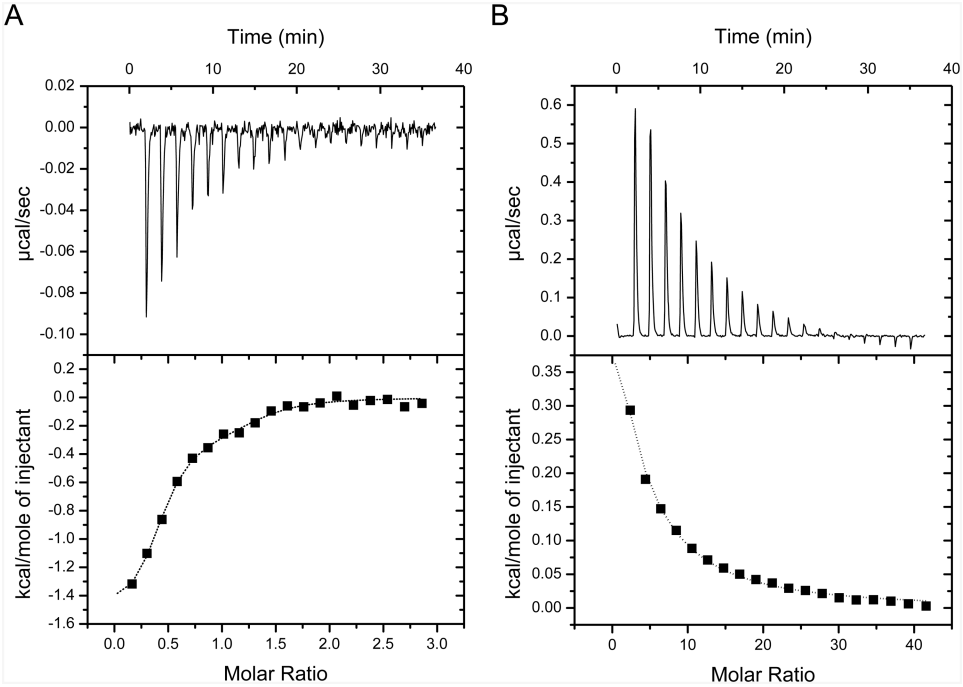

Figure 2.

Isothermal Titration Calorimetry analysis of high- and low-affinity binding of $MgCl_2$ to PP2Cα. All titrations were performed at 25 °C. Bound metals were removed from purified PP2Cα by extensive dialysis against Chelex resin-treated buffers in the presence of excess Chelex resin. In each panel, the raw data are displayed in the upper figure, and the normalized, integrated injection heats are displayed in the lower panel. (A) Analysis of high-affinity sites with the titration of 550 µM $MgCl_2$ into 50 µM PP2Cα. The fitted curve is based on the two-site model. (B) Analysis of the low-affinity site with the titration of 30 mM $MgCl_2$ into 150 µM PP2Cα. The fitted curve is based on the one-site model.

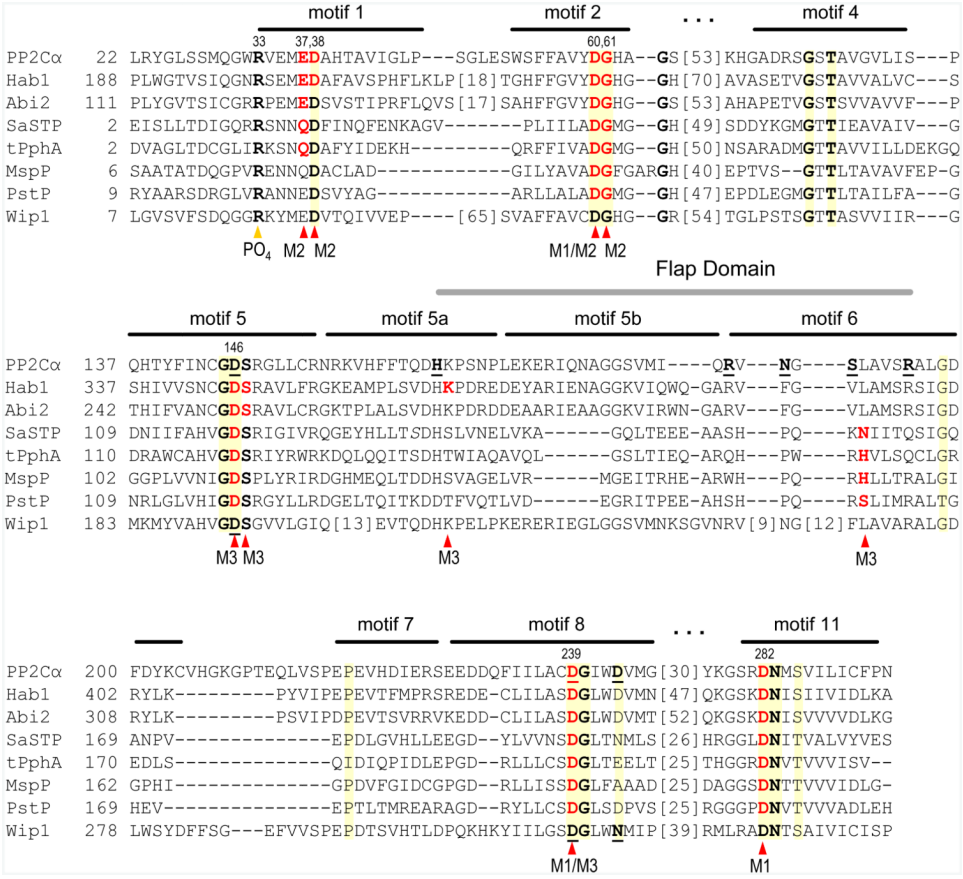

Figure 3.

Multiple sequence alignment of human PP2Cα, Wip1, and several PP2C phosphatases displaying three active site metal ions. Alignment of catalytic domain sequences of seven structurally-characterized PP2C phosphatases was performed using the program MUSCLE (37). The Wip1 sequence was separately aligned (38). Key residues are indicated by PP2Cα residue numbers. Metal ion-coordinating residues are indicated in red. The 15 previously identified highly-conserved residues (4) are indicated by yellow shading. The Flap domain is indicated. Portions of the sequences were omitted for brevity. Mutated residues of PP2Cα and Wip1 discussed in this work are underlined and shown in bold.

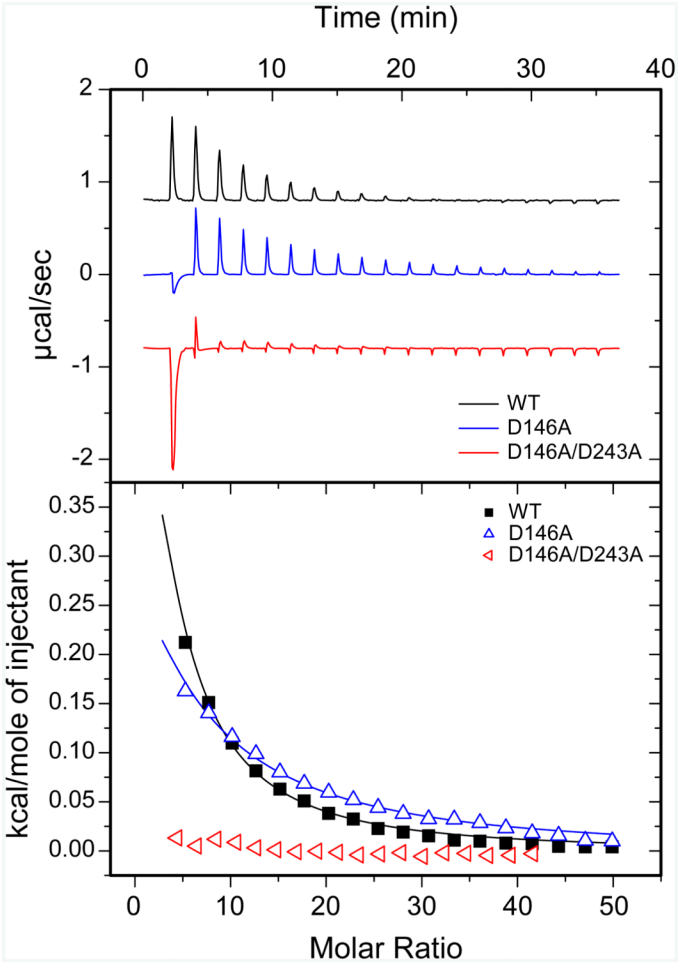

Figure 4.

Isothermal Titration Calorimetry analysis of low-affinity binding of $MgCl_2$ to WT, D146A and D146A/D243A PP2Cα proteins. Titrations were performed at 25 °C with 30 mM $MgCl_2$ titrated into 125-150 µM purified protein solution prepared by extensive dialysis against divalent ion-free buffer. Results shown are representative of two replicates. Upper panel: raw thermograms. The trace for PP2Cα is aligned to the axes; traces for the mutant proteins were shifted vertically for clarity. Lower panel: normalized, integrated injection heats and the best-fit curve based on a one site binding model. The integrated heat of the first injection, which may be influenced by binding of Mg^{2+} ions to the high affinity sites, was not included in the fitting.

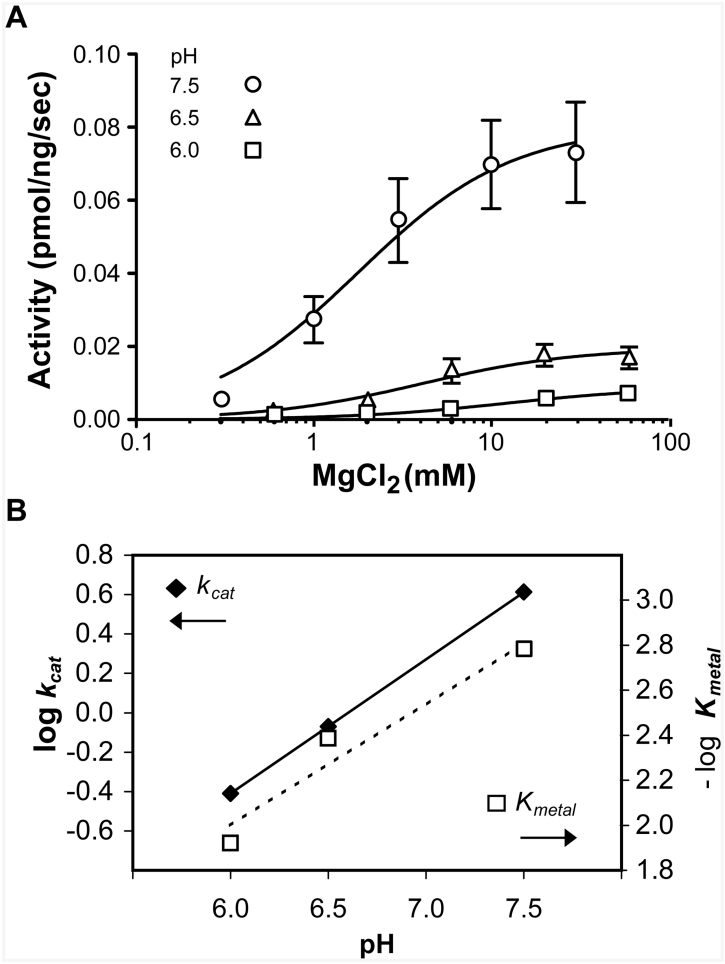

Figure 5.

(A) pH dependence of Mg^{2+}-dependent activation of PP2Cα phosphatase activity. The initial rate of phosphatase activity was measured with 0.3-30 mM $MgCl_2$ in the presence of 100 μM p38α(175-185)(180pT) peptide at 30 °C at the indicated pH values. (B) pH dependence of the catalytic constant, k_{cat} (left axis), and the apparent metal affinity, K_{metal} (right axis).

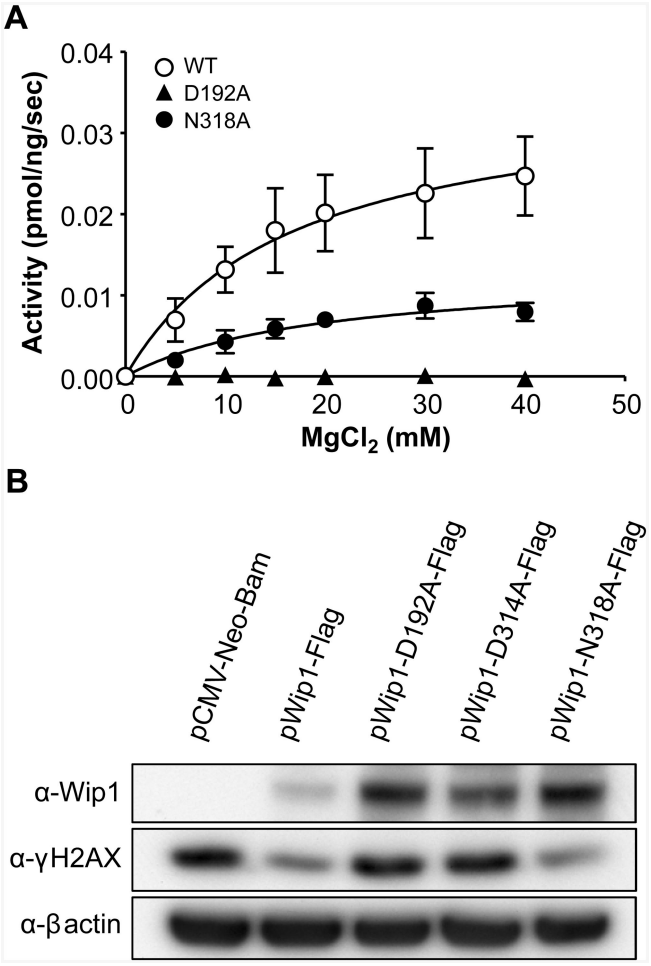

Figure 6.

Mutation of putative third metal coordinating residues reduces or abolishes Wip1 phosphatase activity in vitro and in vivo. (A) $MgCl_2$-concentration dependence of the in vitro phosphatase activity of wildtype and mutant Wip1. Phosphatase activity was measured at 30 °C using 100 μM p38α(175-185)(180pT) peptide in the presence of 0.3-40 mM $MgCl_2$. Each point represents the average of at least three independent measurements. (B) γH2AX level following exposure to IR reports phosphatase activity of WT or mutant Wip1 in vivo. To adjust the level of WT or Wip1 mutant proteins, HEK 293T cells were transfected with a constant total amount of DNA consisting of Wip1-Flag expression vector:parental vector in the following ratios: WT, 1:2; D192A, 1:2; D314A, 1:0.6; N318A, 1:0.2. Transfected cells were exposed to 10 Gy IR and were collected 90 min later. Isolated proteins were analyzed by Western blotting using antibodies specific for Wip1 and H2AX phosphorylated on Ser139 (γH2AX). β-actin served as a loading control.

Table 1

Thermodynamic characterization of the binding of Mg^{2+} to human PP2Cα by isothermal titration calorimetry[a]

Type	Model	*n*	N_n	$K_a/10^6$ M^{-1}	ΔH_n/kcal mol^{-1}	ΔS_n/eu
High affinity[b]	Two sites	1	0.38 ± 0.03	5.9 ± 3.9	−1.56 ± 0.15	25.7
		2	0.90 ± 0.16	0.35± 0.24	−0.30 ± 0.14	24.3
				$K_a/10^3$ M^{-1}		
Low affinity[c]	One site	1	N=1, fixed	0.84 ± 0.03	3.36 ± 0.06	24.6

[a] At 25 °C, in 50 mM HEPES (pH 7.5), 150 mM NaCl, 10% glycerol, 2 mM β-ME. Results given are the means ± SEM of two experiments. Apo-PP2Cα was prepared by dialysis against Chelex resin-treated buffers.

[b] 50μM PP2Cα titrated with 500 μM $MgCl_2$.

[c] 0.15 mM PP2Cα + 0.3 mM $MgCl_2$ titrated with 30 mM $MgCl_2$.

Biochemistry. Author manuscript; available in PMC 2014 August 27.

Table 2

Thermodynamic characterization of low-affinity binding of Mg^{2+} to WT and mutant human PP2Cα by isothermal titration calorimetry[a]

Protein	$K_a/10^3$ M^{-1}	ΔH/kcal mol^{-1}	ΔS/eu	Method(s)[b]
WT	1.85 ± 0.36	2.69 ± 0.46	24 ± 3	EDTA
D146A	0.62 ± 0.20	1.27 ± 0.15	17 ± 0.2	EDTA
D239A	n.d.	n.d.	-	EDTA
D243A	0.63 ± 0.11	2.24 ± 0.37	20 ± 2.4	EDTA
WT	1.39 ± 0.13	3.43 ± 0.27	25.9 ± 1	Dialysis
D146A	0.60 ± 0.05	3.50 ± 0.37	24.5 ± 3	Dialysis
D146A/D243A	n.d.	n.d.	-	Dialysis

[a] At 25 °C, in 50 mM HEPES (pH 7.5), 150 mM NaCl, 10% glycerol, 2 mM β-ME. Results given are the means ± SEM of two or three experiments. n.d., not detected.

[b] In the EDTA method, protein was prepared by dialysis against buffer containing EDTA, then dialyzed extensively against buffer without EDTA or $MgCl_2$. In the Dialysis method, purified protein supplemented with $MgCl_2$ was dialyzed extensively against buffer without $MgCl_2$.

Table 3

Kinetic parameters of WT and active site mutant PP2Cα proteins[a]

	Peptide[b]			pNPP[c]		
Protein	K_m, μM	k_{cat}, s^{-1}	K_{metal}, mM	K_m, mM	k_{cat}, s^{-1}	K_{metal}, mM
WT	27 ± 4	6.3 ± 0.2	1.9 ± 0.3	0.74 ± 0.1	2.3 ± 0.07	3.3 ± 0.5
D146A	n.d.	n.d.	n.d.	n.d.	n.d.	n.d.
D239A	n.d.	n.d.	n.d.	n.d.	n.d.	n.d.
D243A	53 ± 9	5.1 ± 0.3	4.7 ± 1.3	1.3 ± 0.1	3.0 ± 0.1	9.5 ± 1.7
D146A/D243A	n.d.	n.d.	n.d.	n.d.	n.d.	n.d.

[a] Experiments were performed with His tag-free proteins in 50 mM Tris-HCl (pH 7.5), 40 mM NaCl, 0.02% β-ME, and 0.1 mM EGTA at 30 °C.

[b] with 30 mM $MgCl_2$ and 0-400 μM p38α(175-185)(180pT) peptide or 100 μM peptide and 0-30 mM $MgCl_2$; n.d., not detected.

[c] with 10 mM $MnCl_2$ and 0-5 mM pNPP or 5 mM pNPP and 0-30 mM $MnCl_2$; n.d., not detected.

Table 4

Kinetic parameters of WT and Flap domain mutant PP2Cα proteins[a]

	Peptide[b]			pNPP[c]		
Protein	K_m, μM	k_{cat}, s^{-1}	K_{metal}, mM	K_m, mM	k_{cat}, s^{-1}	K_{metal}, mM
WT	49 ± 9	4.6 ± 0.3	1.7 ± 0.3	0.5 ± 0.1	0.68 ± 0.03	1.7 ± 0.3
H164A	144 ± 40	3.2 ± 0.4	4.6 ± 1.5	0.98 ± 0.18	1.3 ± 0.1	3.2 ± 0.6
R186A	n.d.	n.d.	n.d.	1.1 ± 0.2	2.7 ± 0.2	2.0 ± 0.4
N188A	n.d.	n.d.	n.d.	0.7 ± 0.1	1.4 ± 0.1	1.8 ± 0.3
S190A	49 ± 9	4.3 ± 0.3	1.9 ± 0.3	0.55 ± 0.2	0.65 ± 0.07	3.3 ± 0.4
S190T	46 ± 7	5.1 ± 0.3	2.3 ± 0.3	0.29 ± 0.05	0.44 ± 0.02	3.9 ± 0.8
R195A	n.d.	n.d.	n.d.	0.86 ± 0.2	0.16 ± 0.01	2.3 ± 0.5

[a] Experiments were performed with His-tagged proteins in 50 mM Tris-HCl (pH 7.5), 0.02% β-ME, and 0.1 mM EGTA at 30 °C.

[b] Experiments were performed with 30 mM $MgCl_2$ and 0-400 μM p38α(175-185)(180pT) peptide or 100 μM peptide and 0-30 mM $MgCl_2$; n.d., not detected.

[c] Experiments were performed with 10 mM $MnCl_2$ and 0-5 mM pNPP or 5 mM pNPP and 0-30 mM $MnCl_2$; n.d., not detected.

Table 5

Metal ion type- and concentration-dependence of PP2Cα phosphatase activity[a]

Metal ion(s)	K_{metal}, mM	k_{cat}, s^{-1}
$MgCl_2$[b]	1.7 ± 0.3	4.6 ± 0.3
$MgCl_2$ plus 0.1 mM $MnCl_2$	13± 4.2	3.6 ± 0. 5
$MnCl_2$	1.4 ± 0.5	0.16 ± 0.01
$MnCl_2$ plus 0.1 mM $MgCl_2$	1.3 ± 0.5	0.13 ± 0.01

[a] Experiments were performed with His-tagged PP2Cα in 50 mM Tris-HCl (pH 7.5), 0.02% β-ME, and 0.1 mM EGTA, 40 mM NaCl, 100 μM p38α (175-185)(180pT) peptide and 0 to 30 mM of the indicated salt, with or without 0.1 mM of the alternative salt, at 30 °C.

[b] Results from Table 4.